A 3D Printed 140 GHz Multifocal Dielectric Transmitarray Antenna for 2D Mechanical Beam-Scanning

Jiexin Lai, *Student Member, IEEE*, Xiaojing Lv, *Member, IEEE,* and Yang Yang, *Senior Member, IEEE*

***Abstract*—In this work, a 3D printed multifocal all-dielectric transmitarray antenna (TAA) is proposed for two-dimensional (2D) beam-scanning at 140 GHz. Taking advantage of the TAA element phase shifting by varying incident angles, the proposed TAA can meet the phase compensation requirement for the feed beams from multiple ports with different incident angles. The genetic algorithm (GA) is employed to optimise the phase distribution at the sub-terahertz band. The measured 3-dB gain bandwidths of the proposed TAA are 14.3%. By mechanically rotating the feed horn, the multifocal TAA can realise a measured peak gain of 26.6 dBi at 140 GHz with a higher gain improvement of 12 dB and a ±30° beam-scanning range and 2.1 dB scan loss in E-plane, H-plane, and D-plane (Diagonal-plane, ϕ=45°). The proposed TAA demonstrates a broadband 2D mechanical beam-scanning performance in the sub-terahertz band.**

***Index Terms*—Transmitarray antenna (TAA), multifocal, 2D mechanical beam-scanning, terahertz, 3D printing, genetic algorithm.**

I. INTRODUCTION

Broad-range beam-scanning is among the most desirable features in the trending terahertz (THz) telecommunications systems. Aiming for extensive coverage with high gain, transmitarray antennas (TAAs) and lens antennas (LAs) have attracted much attention. Over the last decade, existing unifocal [1], bifocal [2,3] and multifocal [4-6] beam-scanning TAAs and LAs are designed based on geometric optics (GO) analysis and the Fresnel formula. Their performance is dependent on the degrees of freedom (DOFs), which include the positioning and tilt angles of the feeding sources, as well as the shape of the phase distribution (PD).

Overall, there are three main types of mechanical beam-scanning or electronic scanning TAA or LA. Fig. 1 (a) illustrates a TAA with a focal plane [7], which has the strength of a wide beam-scanning range. To cover the radiation of all the feeding sources, the panel size of this TAA tends to be large [8,9]. Therefore, the aperture efficiency (AE) and a lower focal-to-diameter ratio (F/D) are compromised. The shape of the phase distribution needs to be elliptical for a wider one-dimensional (1D) beam-scanning range. A 2D gradient index (GRIN) lens [10] with limited DOFs of the PD can only srealise −20° to 20° range. TAAs [11] with a focal locus in Fig. 1(b) fully utilise the DOF of the feeding sources, which can achieve a wide coverage. Recently, a 2D beam-scanning lens with a ±45° range has been proposed [12,13]. The focal length and the direction angle of each feeding source are different. TAAs with a focal arc [14,15] in Fig. 1 (c) can achieve a high AE, and wide coverage, and the beam deviation factor (BDF) is equal to 1, which is defined as the ratio between the main beam direction and the feeding source tilt angle. In addition, the focal-to-diameter ratio (F/D) is also important. With the same reasonable focal lengths, smaller F/D increase the difficulty of designing beam-scanning transmiarrays, but it can realise a higher gain improvement compared with the feed source antenna.

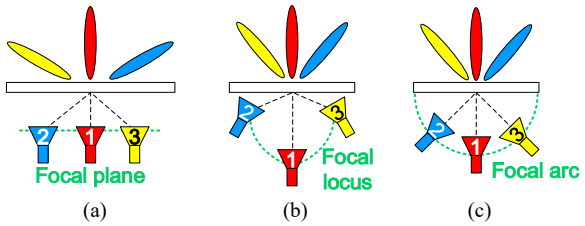

(a) (b) (c)

Fig. 1. Schematics of the beam-scanning transmitarray. (a) TAA with a focal plane; (b) TAA with a focal locus; (c) TAA with a focal arc.

Due to the strong flexibility of the 3D printing technology, there have been various all-dielectric transmitarrays and reflectarrays in the open literature [16,17], including the circularly polarised transmitarray [18], the THz near-field beam-scanning lens [19] and THz OAM generator [20]. 3D printed dielectric TAA [21] can achieve 21.5 % relative bandwidth at 1dB level by adding the truncated pyramid hole. In [22], by considering the oblique incidences, the all-dielectric TAA realise gain improvement of 4.5 dB at 26 GHz with a short focal length of $1.73\lambda_0$.

This letter presents a genetic algorithm (GA) optimisation method suitable for a large focal length or small focal-to-diameter ratio (F/D) transmitarrays to achieve a high gain improvement with a ±30° beam-scanning capability. It also benefits from an additional DOF for optimisation, positioning the rotation centre of the feeding sources. By utilising the TAA element phase shifting with varying incident angles, the proposed TAA can meet the phase compensation requirement for the feed beams from multiple ports and srealises higher gain improvement of 12 dB with a continuous

Manuscript received XX, 2023. This work was supported by Australian Research Council (ARC) Linkage Infrastructure Equipment and Facilities (Grant No. LE220100035) and Linkage Project (Grant No. LP210300004), in part by the New South Wales Space Research Network Pilot Project. *(Corresponding author: A/Prof. Yang Yang).*

Jiexin Lai, Xiaojing Lv and Yang Yang are with school of Electrical and Data Engineering, University of Technology Sydney, Ultimo, NSW 2007, Australia.

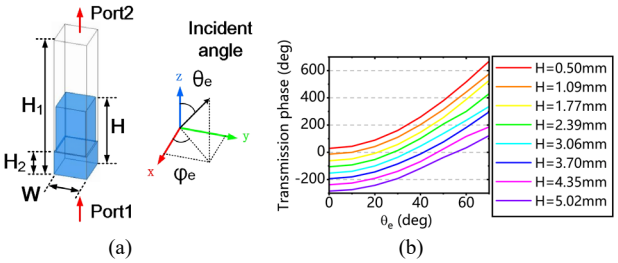

Fig. 2. Proposed method of TAA element transmission phase shifting by varying incident angles: (a) Element configuration. ($H1 = 6mm, H2 = 0.5mm, W = 1\ mm, H$ is variable). (b) Transmission phase varies with incident angle (θ_e) at 140 GHz.

2D beam-scanning from $-30°$ to $30°$ in E-plane, H-plane, and D-plane (Diagonal-plane, $\phi = 45°$). The proposed TAA obtains a maximum measured aperture efficiency of 43.1%. The broadband performance of the dielectric elements makes the TAA achieve the 14.3 % 3-dB gain bandwidth.

II. Transmitarray Design

A. Dielectric Element

The TAA element in Fig. 2 (a) is simulated by using ANSYS High-Frequency Structure Simulation (HFSS). A dielectric square pole with a width W and a variable height H is made by 3D printing material, Cyclic Olefin Copolymer (COC), with relative permittivity constant of 2.34 and a loss tangent of 0.00017 at THz-band [23]. It should be noted that the H_1 is the total height of the transmitarray element which contains both air and dielectric; the height of the base is H_2, and the H is the height of the dielectric pole. By changing the height H of the element (ranging from H_1 to H_2), the element can realise a phase shift across the full phase cycle (2π) [24]. There is a $0.1\ mm$ air gap between the pillars to prevent the modeling error in HFSS. In Fig. 2 (b), the phase response for different incident angles needs to be considered, transmission phases against different incident angles θ_e are shown, with varying element heights H.

The incidence angle effect [25] has been considered in designing reflectarray antennas (RAAs). As for TAAs, the influence of incident angle can be shown in Fig. 2(c). To obtain the relationshop between the transimission phase and the incident angle, eight curvilinear equations need to be extracted and utilised in PDs calculation. By using MATLAB basic fitting tool, the cubic curve fitting equation coefficients are obtained, and their corresponding coefficients are shown in Table I, where φ_{trans} is the transmission phase and θ_e represents the incident angle, element 1 corresponds to $H = 5.02\ mm$ in Fig. 2 (c), while element 2 refer to $H = 4.35\ mm$ and so on. Additionally, the increase in φ_e (Fig. 2 (a)) has little effect on the transmission phase. Therefore, φ_e is equal to 0° in this case.

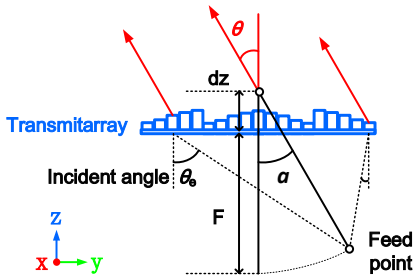

Fig. 3. Coordinate system of the proposed TAA.

B. Principle

A 25×25 TAA is employed to demonstrate the principle by using the coordinate system shown in Fig. 3, where the focal length is F, dz is the offset of the feeding source rotation centre, and α is the rotation angle of the feeding source and (θ) is the radiation beam direction. By default, the feeding source is coplanar with the beam. The PD of the TAA is based on Fermat' s principle. The input PD for each element can be given by:

$$\varphi_{ij} = k_0\left(\sqrt{\left(x_{ij} - x_F\right)^2 + \left(y_{ij} - y_F\right)^2} - (F - z_F)\right) \quad (1)$$

where k_0 is the wave number in free space, and (x_F, y_F, z_F) represents the position of the feeding source, and (x_{ij}, y_{ij}) is the position of the transmitarray element. Regarding the TAA, the incident angle of the i, j th element $\theta_{e\,ij}$ can be given by:

$$\theta_{e\,ij} = \left|\arctan\left(\frac{\sqrt{\left(x_{ij} - x_F\right)^2 + \left(y_{ij} - y_F\right)^2}}{F - z_F}\right)\right| \quad (2)$$

TABLE I

Transmission Phase (φ_{trans}) vs. Incident Angel (θ_e) by Cubic Curve Fitting Equation (φ_{trans}=A*$\theta_e{}^3$+B*$\theta_e{}^2$+C*θ_e+D)

Element	1(H=5.02mm)	2(H=4.35mm)	3(H=3.7mm)	4(H=3.06mm)	5(H=2.39mm)	6(H=1.77mm)	7(H=1.09mm)	8(H= 0.5mm)
A	-0.00083	-0.00117	-0.00034	-0.00089	-0.00075	-0.00042	-0.00063	-0.00054
B	0.148068	0.186158	0.119518	0.166241	0.164166	0.153432	0.169227	0.172056
C	-0.486	-1.22129	0.305155	-0.30907	-0.19753	-0.22715	-0.33878	-0.28517
D	-284.45	-235.344	-194.466	-152.824	-106.515	-62.1204	-13.8539	29.78446

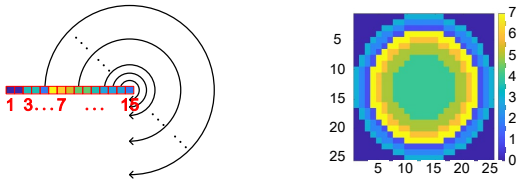

(a) (b)

Fig. 4. GA-based 2D multifocal TAA_2. (a) Rotation of a row of elements. (b) Optimal PD.

The transmission phase can be calculated using the equation from Table I.

$$\varphi_{trans,ij} = f(\theta_{e\,ij}) \tag{3}$$

Thus, the calculated PD is given by

$$\varphi_{cal,ij} = \varphi_{ij} - \varphi_{trans,ij} \tag{4}$$

To obtain a tilting beam angle, the i, j th ideal output PD can be given by:

$$\varphi_{ideal,ij} = k_0\, y_{ij}\, sin\theta \tag{5}$$

$$\varphi_{ideal,ij} = mod(\varphi_{ideal,ij} + \varphi_0, 360°) \tag{6}$$

where k_0 represents the wave number, (θ, φ) indicates the angle of the radiation beam, and φ_0 is the additional phase which does not affect the main beam direction. The ultimate purpose is to make φ_{cal} close to φ_{ideal}. In this case, there are four output PDs φ_{cal}, when $\alpha = 0°$, $\alpha = 10°$, $\alpha = 20°$,and $\alpha = 30°$. Their corresponding PDs φ_{ideal} are related to $\theta = 0°$, $\theta = 10°$, $\theta = 20°$, and $\theta = 30°$.

C. Optimisation

Genetic algorithm (GA) [26,27] has been used in designing an ultrawideband TAA or LA. It can also be used to optimise the elements to fit the dielectric element in a multifocal TAA. However, there are some restrictions to optimisation. As shown in Fig. 4 (a), to realise centrosymmetric PD, a row of elements rotates around the centre to generate a 2D PD in Fig. 4 (b), and the dark blue parts except the circle are set to 0. This process can reduce the number of optimisation parameters instead of optimising an entire matrix, which can reduce the computational load. The population size is 120, and the generation is 150 in the GA-based optimisation. These elements' series numbers are integer variables to be optimised. The parameters of 'dz' and 'F' are also included in the optimisation parameters. The cost function is set as an average difference between the calculated and ideal phase for all the elements. There are four ideal PDs for $\theta = 0°$, $\theta = 10°$, $\theta = 20°$, and $\theta = 30°$. Thus their corresponding initial phases φ_0 are also set as the optimisation parameters.

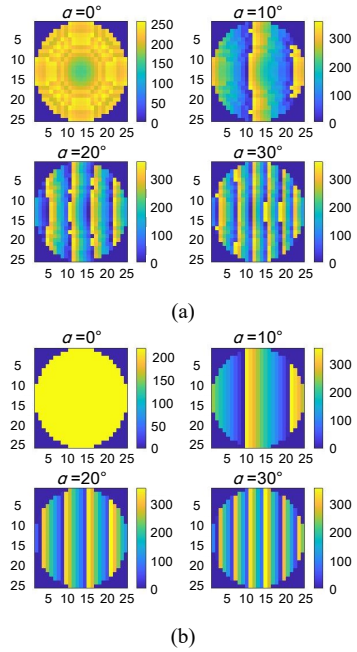

(a)

(b)

Fig. 5. GA-based multifocal transmitarray PDs. (a) Calculated output PDs of the proposed TAA, (b) Ideal output PDs..

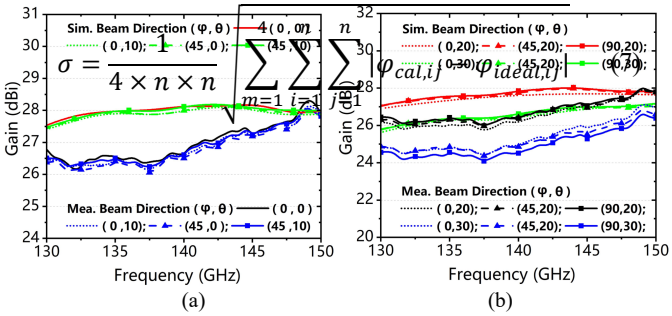

(a) (b)

Fig. 6. Simulated and measured peak gain for different scanning angles when (a) $\theta = 0°$, $\theta = 10°$, (b) $\theta = 20°$, and $\theta = 30°$.

$$\sigma = \frac{1}{4 \times n \times n} \sum_{m=1}^{4} \sum_{i=1}^{n} \sum_{j=1}^{n} \varphi_{cal,ij}(\varphi_{ideal,ij}) \tag{7}$$

where $n = 25$ is the dimension of the TAA, and m represents the four beam directions ($\theta = 0°$, $\theta = 10°$, $\theta = 20°$, and $\theta = 30°$). The optimised element series is [3, 2, 1, 7, 6, 5, 5, 4, 4, 4, 4, 4], which corresponds to the phase transmission in Fig. 4 (b). The optimal focal length 'F' and the centre offset 'dz' are 24.2 mm and 3.9 mm. The additional phases φ_0 for $\theta = 0°$, $\theta = 10°$, $\theta = 20°$, and $\theta = 30°$ are 221.9°, 243.6°, 91.9°, and 167.3°, respectively. The PD comparisons are shown in Fig. 5. The PDs in Fig. 5 (a) are obtained by calculating equation (4), while the ideal PDs in Fig. 5 (b) are from equation (6).

III. Experiments and Comparisons

A. Experiments

The far-field measurement setup consists of a Keysight PNA Network Analyzer N5225B, a VDI WR 6.5 extension module transmitter (D-band, 110 – 170 GHz) , and a VDI WR 6.5 extension module receiver. The gain of the feed horn is about 14 dBi. The aperture size is about $12.5^2\pi\ mm^2$, the focal

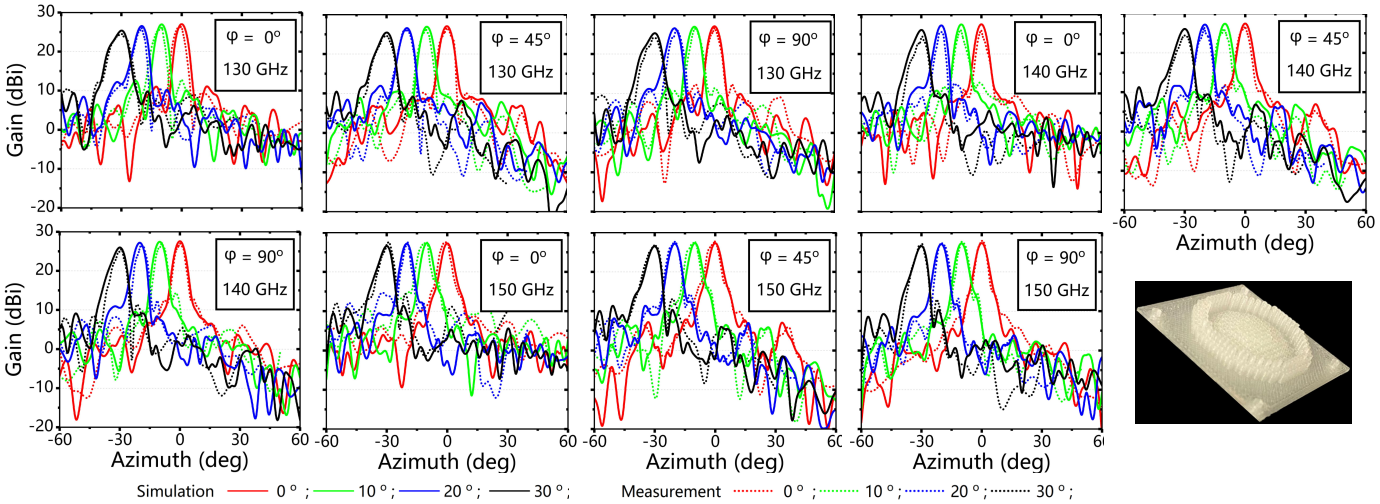

Fig. 7. Simulated and measured beam steering radiation patterns at 130 GHz, 140 GHz, and 150 GHz

length is 24.2 mm, and the offset of the centre is 3.9 mm in HFSS, and the focal-to-diameter (F/D) ratio is 0.83.

The simulated and measured peak gains at different scanning angles are given in Fig. 6. The peak gains with the same θ are almost equal. The simulated peak gains of $\theta = 0°$ and $\theta = 10°$ from 27.4 to 28.2 dBi, and that of $\theta = 20°$ and $\theta = 30°$ are from 27.0 to 28.0 dBi and from 25.6 to 27.2 dBi. The measured peak gains are from 26.5 to 28.0 dBi ($\theta = 0°$), from 26.1 to 27.8 dBi ($\theta = 10°$), from 26.3 to 28.0 dBi dBi ($\theta = 20°$), and from 24.7 to 26.2 dBi ($\theta = 30°$). Fig. 7 shows the simulated and measured beam-scanning radiation patterns at 130 GHz, 140 GHz, and 150 GHz in the E-plane (φ=0°), D-plane (φ=45°), and H-plane (φ=90°). The simulated and measured cross-polarisation is 30-40 dB lower than the co-polarisation. Thus, they are omitted for brevity. The simulated gains of the TAA at 140 GHz are from 26.6 to 28.1 dBi with a scan loss of about 1.5 dB, while the measured ones are from 24.5 to 26.6 dBi with a scan loss of 2.1 dB. This means the proposed dielectric lens realises a 2D beam-scanning performance within ±30° from the frequency of 130 GHz to 150 GHz.

B. Comparisons

The proposed transmitarray is compared with other relevant state-of-the-art designs in Table II. Since measured results can be affected by fabrication tolerance and experimental setup, to be fair, we only compare the simulated results of our proposed design to simulations of those in the literature with experimental validation. Due to a lower focal length and a large F/D, TAAs in [12,13] realise high AE and wide scanning range, but the gain improvement compared to the feeding source is limited. In [15], by using a tapered matching structure, the transmission phase of the elements is not sensitive to the incident angles. Whereas the proposed design can realise high gain improvement (about 14.1 dB in simulation) and ±30° 2D beam scanning performance. Nevertheless, the measured gain experiences 1-2 dB reduction due to fabrication error.

IV. Conclusion

In summary, a sub-THz multifocal dielectric TAA for 2D mechanical beam-scanning is presented. By using the proposed optimisation method, the proposed TAA can better gain improvement. On the other hand, wide-angle beam-scanning capability is also maintained. It is suitable for a large focal length or small focal-to-diameter ratio (F/D) transmitarray. The beams are tilted at 0°, 10°, 20°, and 30° at E/D/H plane. the proposed TAA is a promising candidate for the future THz communication application because of the 2D beam-scanning performance, high gain and high AE, and lower fabrication cost.

TABLE II
COMPARISONS WITH OTHER MECHANICAL BEAM-SCANNING TRANSMITARRAYS

Ref	Freq. (GHz)	Gain (dBi)	Source Gain (dBi)	Gain Impv. (dB)	AE (%)	D*(λ_0)	F*(λ_0)	F/D	Scan range	Scan loss (dB)
[12]	13	21.9	17.5	4.4	64.31	4.94	3.64	0.73	±45° (2D)	2.6
[13]	190	29.6	22	7.6	35.7	14.2	35.2	2.48	±48° (1D)	1.4~4
[15]	30	29.97	17	12.97	35.12	15	15	1	±30° (1D)	2.9
This work	140	28.1	14	14.1	48.06	11.67	11.25	0.96	±30° (2D)	1.5

D* : Diameter; F* : Focal length

REFERENCE

[1] P. Mei, G. F. Pedersen and S. Zhang, "Performance improvement of mechanically beam-steerable transmitarray antennas by using offset unifocal phase symmetry," in *IEEE Transactions on Antennas and Propagation*, vol. 71, no. 1, pp. 1129-1134, Jan. 2023.

[2] P. Nayeri, F. Yang and A. Z. Elsherbeni, "Bifocal design and aperture phase optimisations of reflectarray antennas for wide-angle beam scanning performance," in *IEEE Transactions on Antennas and Propagation*, vol. 61, no. 9, pp. 4588-4597, Sep.. 2013.

[3] L. Peebles, "A dielectric bifocal lens for multibeam antenna applications," in *IEEE Transactions on Antennas and Propagation*, vol. 36, no. 5, pp. 599-606, May 1988.

[4] P. -Y. Feng, S. -W. Qu, X. -H. Chen and S. Yang, "Low-profile high-gain and wide-angle beam scanning phased transmitarray antennas," in *IEEE Access*, vol. 8, pp. 34276-34285, 2020.

[5] G. -B. Wu, S. -W. Qu and S. Yang, "Wide-angle beam-scanning reflectarray with mechanical steering," in *IEEE Transactions on Antennas and Propagation*, vol. 66, no. 1, pp. 172-181, Jan. 2018.

[6] G. -B. Wu, S. -W. Qu, S. Yang and C. H. Chan, "Low-cost 1-D beam-steering reflectarray with ±70° scan coverage," in *IEEE Transactions on Antennas and Propagation*, vol. 68, no. 6, pp. 5009-5014, June 2020.

[7] Á. F. Vaquero et al., "Design of low-profile transmitarray antennas with wide mechanical beam steering at millimeter waves," in *IEEE Transactions on Antennas and Propagation*, vol. 71, no. 4, pp. 3713-3718, April 2023.

[8] E. B. Lima, S. A. Matos, J. R. Costa, C. A. Fernandes and N. J. G. Fonseca, "Circular spolarisation wide-angle beam steering at ka-band by in-plane translation of a plate lens antenna," in *IEEE Transactions on Antennas and Propagation*, vol. 63, no. 12, pp. 5443-5455, Dec. 2015.

[9] T. K. Pham, L. Guang, D. González-Ovejero and R. Sauleau, "Dual-band transmitarray with low scan loss for satcom applications," *in IEEE Transactions on Antennas and Propagation*, vol. 69, no. 3, pp. 1775-1780, March 2021.

[10] W. Shao and Q. Chen, "2-D beam-steerable sgeneralised Mikaelian lens with unique flat-shape characteristic," in *IEEE Antennas and Wireless Propagation Letters*, vol. 20, no. 10, pp. 2033-2037, Oct. 2021.

[11] L. -Z. Song, P. -Y. Qin, S. -L. Chen and Y. J. Guo, "An elliptical cylindrical shaped transmitarray for wide-angle multibeam applications," in *IEEE Transactions on Antennas and Propagation*, vol. 69, no. 10, pp. 7023-7028, Oct. 2021,.

[12] L. -Z. Song, M. Ansari, P. -Y. Qin, S. Maci, J. Du and Y. Jay Guo, "2-D wide-angle multi-beam flat GRIN lens with a high aperture efficiency," in *IEEE Transactions on Antennas and Propagation*., Early Access.

[13] L. -Z. Song, T. Zhang, J. -X. Lai, Y. Yang and J. Du, "A 180 GHz to 220 GHz wideband transmitarray with wide-angle beam steering for intersatellite communications," in *IEEE Transactions on Antennas and Propagation*, Early Access

[14] P. Nayeri, F. Yang and A. Z. Elsherbeni, "Design of multifocal transmitarray antennas for beamforming applications," *2013 IEEE Antennas and Propagation Society International Symposiu*m (APSURSI), Orlando, FL, USA, 2013, pp. 1672-1673.

[15] Massaccesi A, Dassano G, Pirinoli P. Beam scanning capabilities of a 3d-printed perforated dielectric transmitarray. in *Electronics*, vol. 8, no. 4, pp. 379-392, Mar 2019

[16] S. A. Matos et al., "3-D-printed transmit-array antenna for broadband backhaul 5g links at V-band," in *IEEE Antennas and Wireless Propagation Letters*, vol. 19, no. 6, pp. 977-981, June 2020.

[17] J. Zhu, Y. Yang, D. Mcgloin, S. Liao and Q. Xue, "3-D printed all-dielectric dual-band broadband reflectarray with a large frequency ratio," in *IEEE Transactions on Antennas and Propagation*, vol. 69, no. 10, pp. 7035-7040, Oct. 2021.

[18] F. Wei, J. -W. Hao, L. Xu and X. Shi, "A circularly spolarised 3-D printed dielectric transmitarray antenna at millimeter-wave band," in *IEEE Antennas and Wireless Propagation Letters*, vol. 20, no. 7, pp. 1264-1268, July 2021.

[19] G. -B. Wu, K. F. Chan, S. -W. Qu and C. H. Chan, "A 2-D beam-scanning bessel launcher for terahertz applications," in *IEEE Transactions on Antennas and Propagation*, vol. 68, no. 8, pp. 5893-5903, Aug. 2020.

[20] G. -B. Wu, K. F. Chan and C. H. Chan, "3-D printed terahertz lens to generate higher order bessel beams carrying OAM," in *IEEE Transactions on Antennas and Propagation*, vol. 69, no. 6, pp. 3399-3408, June 2021.

[21] A. Massaccesi et al., "3D-printable dielectric transmitarray with enhanced bandwidth at millimeter-waves," in *IEEE Access*, vol. 6, pp. 46407-46418, 2018.

[22] Y. Cai, P. Mei, X. Q. Lin and S. Zhang, "A sgeneralised method for gain bandwidth enhancement of transmitarray antennas considering oblique incidences," in *IEEE Transactions on Circuits and Systems II: Express Briefs*, Early Access.

[23] Mavrona E, Graf J, Hack E, et al. sOptimised 3D printing of THz waveguides with cyclic olefin copolymer[J]. *Optical Materials Express*, 2021, 11(8): 2495-2504.

[24] H. Yi, S. -W. Qu, K. -B. Ng, C. H. Chan and X. Bai, "3-D printed millimeter-wave and terahertz lenses with fixed and frequency scanned beam," in *IEEE Transactions on Antennas and Propagation*, vol. 64, no. 2, pp. 442-449, Feb. 2016.

[25] E. R. F. Almajali and D. A. McNamara, "Angle of incidence effects in reflectarray antenna design: making gain increases possible by including incidence angle effects," in *IEEE Antennas and Propagation Magazine*, vol. 58, no. 5, pp. 52-64, Oct. 2016.

[26] X. Liu et al., "Ultrabroadband all-dielectric transmitarray designing based on genetic algorithm soptimisation and 3-D print technology," in *IEEE Transactions on Antennas and Propagation*, vol. 69, no. 4, pp. 2003-2012, April 2021.

[27] W. -s. Yu, L. Peng, Y. -f. Liu, Q. -x. Zhao, X. Jiang and S. -m. Li, "An ultrawideband and high-aperture-efficiency all-dielectric lens ant enna," in *IEEE Antennas and Wireless Propagation Letters*, vol. 20, no. 12, pp. 2442-2446, Dec. 2021.